Observation of nearly identical superconducting transition temperatures in the pressurized Weyl semimetal MIrTe$_4$ (M=Nb and Ta)

Sijin Long[1,4]*, Shu Cai[1]*, Rico Schönemann[2], Priscila F. S. Rosa[2], Luis Balicas[3], Cheng Huang[1,4]
Jing Guo[1,6], Yazhou Zhou[1], Jinyu Han[1,4], Liqin Zhou[1,4], Yanchun Li[5], Xiaodong Li[5],
Qi Wu[1], Hongming Weng[1,4], Tao Xiang[1,4,6] and Liling Sun[1,4,6]†

[1]*Institute of Physics, National Laboratory for Condensed Matter Physics, Chinese Academy of Sciences, Beijing, 100190, China*
[2]*MPA-MAGLAB, Los Alamos National Laboratory, Los Alamos, New Mexico 87545, USA*
[3]*National High Magnetic Field Laboratory, Tallahassee, Florida 32310, USA*
[4]*University of Chinese Academy of Sciences, Department of Physics, Beijing 100190, China*
[5]*Institute of High Energy Physics, Chinese Academy of Science, Beijing 100049, China*
[6]*Songshan Lake Materials Laboratory, Dongguan, Guangdong 523808, China*

Here we report the observation of pressure-induced superconductivity in type-II Weyl semimetal (WSM) candidate NbIrTe$_4$ and the evolution of its Hall coefficient (R_H), magnetoresistance (MR), and lattice with increasing pressure to ~ 63 GPa. These results provide a significant opportunity to investigate the universal high-pressure behavior of ternary WSMs, including the sister compound TaIrTe$_4$ that has been known through our previous studies. We find that the pressure-tuned evolution from the WSM to the superconducting (SC) state in these two compounds exhibit the same trend, *i.e.*, a pressure-induced SC state emerges from the matrix of the non-superconducting WSM state at ~ 27 GPa, and then the WSM state and the SC state coexist up to 40 GPa. Above this pressure, an identical high-pressure behavior, characterized by almost the same value of R_H and MR in its normal state and the same value of T_c in its SC state, appears in both compounds. Our results not only reveal the evolution from the WSM state to the SC state, but also demonstrate that NbIrTe$_4$ and TaIrTe$_4$ can make the same contribution to the normal and SC states that inhabit in the high-pressure phase, although these two compounds have dramatically different band structure at ambient pressure.

Weyl semimetals (WSMs) have recently attracted extensive attention in the field of condensed matter physics and material science since Weyl fermions have not been observed so far as a fundamental particle in high energy physics [1-5]. In condensed matter physics, the Weyl semimetal is accepted as a topologically nontrivial metallic phase, where Weyl fermions emerge as quasiparticles from linear crossing bands [1, 6, 7]. Two types of WSMs have been predicted theoretically [1, 8-11] and identified experimentally [3, 12, 13]. The materials of *MX* (*M* = Ta, Nb and *X* = As, P) are classified as type-I WSMs, characterized by a point-like Fermi surface at the Weyl node. While type-II WSMs can be found in the transition-metal dichalcogenide family, which includes the compounds of MTe_2 as well as MP_2 (*M*=W, Mo) and the ternary variants of $MXTe_4$ (*M* = Ta, Nb; X = Ir, Rh) [5, 11, 14-16]. The electronic structure of the WSMs gives rise to fascinating phenomena in transport properties, such as a chiral anomaly in the presence of parallel electric and magnetic fields leading to negative magnetoresistance, a novel anomalous Hall response, surface-state quantum oscillations and exotic superconductivity [17-24]. These properties of the WSMs establish them as a new platform for exploring potential applications in nonlinear optics.

Similar to the lattice structure of $TaIrTe_4$, $NbIrTe_4$ also crystallizes in an orthorhombic (OR) unit cell with the $Pmn2_1$ space group and can be viewed as a cell-doubling derivative [5, 15]. Theoretical calculations indicate that $NbIrTe_4$ has a more complicated electronic structure (16 Weyl points in the Brillouin zone) [5] than $TaIrTe_4$ (4 Weyl points in the Brillouin zone) [15, 25]. The presence of Weyl points in

$NbIrTe_4$, accompanied by the common features of a large non-saturating *MR* effect, have been supported experimentally [26]. Pressure is an important tuning parameter that can be utilized to alter the lattice and corresponding electronic structures of a material and therefore influence its electrical transport properties. It is our goal to gain a deeper insight into the nature of Weyl semimetals and in particular to achieve a better understanding of the connection between its nontrivial WSM and SC states. Compelling examples of pressure-induced superconducting transition have been observed in the type-II WSM WTe_2 [27, 28], T_d-$MoTe_2$ and $MoTe_{2-x}S_x$, [20, 29, 30]. As a ternary variant of WTe_2, $TaIrTe_4$ has also displayed superconductivity at high pressures [31] and surface superconductivity [32]. The high-pressure behavior of the new WSM $NbIrTe_4$ remains unknown, and the connection between the WSM and SC states in the ternary WSMs as a function of lattice changes is an open question. In this work, we reveal the evolution of pressure-induced superconductivity from the ambient pressure WSM state in $NbIrTe_4$ and compare our results with those observed in $TaIrTe_4$.

High-quality single crystals of $NbIrTe_4$ were grown by a Te flux method as described in [26]. The scanning electron microscope (SEM) mapping and energy dispersive spectrometer (EDS) analysis on the $NbIrTe_4$ single crystal were carried out before high pressure experiments. The results of the SEM mapping show that the constituent elements (Nb, Ir and Te) distribute homogeneously in the single crystal (see Supplementary Material [33]). The EDS analysis shows that the stoichiometry of the sample used for this study is Nb1: Ir0.96: Te4.04 (see Supplementary Material [33]), very close to the 1:1:4 stoichiometry. Figures 1a and 1b show the temperature *(T)* dependence of the electrical resistance (R) measured in a $NbIrTe_4$ sample (S#1) under pressures to 54.8 GPa within the temperature range of 1.5- 300 K. Over the pressure range investigated, *R(T)* displays metallic behavior as observed at ambient pressure. The details of the high-pressure measurements on the S#1 can be found in the Supplementary Material [33]. The pressure for measurements was determined by the ruby fluorescence method [34] and the shift of diamond Raman [35, 36]. Considering the anisotropic transport property of the *M*IrTe4 (*M*=Ta and Nb), *i.e.* the resistance along b axis (R_b) is much higher than that along a axis (R_a) [37], in the studies on the sample 2 (S#2), we not only ascertained the crystal orientation before loading the sample into the high-pressure cell, but also adopted the standard-four-electrode method for getting reliable data (see the geometry of standard-four-probe method in the Supplementary Material [33]). The resistance measurements on the S#2 was performed in a ^{3}He cryostat down to 0.35 K. A resistance drop with the transition temperature of ~0.69 K is found at 27.2 GPa (Fig.1c). Upon further compression, a zero-resistance state is observed at pressures around 32.4 GPa (Fig. 1c), indicating a superconducting transition. The transition temperature increases with pressure and reaches 1.94 K at 54.6 GPa. To further characterize whether the pressure-induced resistance drop is associated with a superconducting transition, we applied a magnetic field along the inter planar direction at 57 GPa. As shown in Fig. 1d, the transition shifts to lower temperatures upon increasing the magnetic field, indicating that the observed resistance drop indeed originates from a superconducting transition. We estimated the upper critical magnetic field (H_{c2}) for the superconducting phase of $NbIrTe_4$ by using the Werthamer-Helfand-

Hohenberg (WHH) formula [38]: $H_{C2}^{\mathrm{WHH}}(0)=-0.693T_c(dH_{C2}/dT)_{T=Tc}$, which yields an upper critical field of about 1.2 T at 57 GPa (inset of Fig. 1d). We repeated the measurements on a new sample (S#3) in the same experimental manner as that of the sample 2 (S#2) and found that the pressure-induced superconducting transition in $NbIrTe_4$ is reproducible (Fig. 1e and 1f, as well as Supplementary Material). The superconducting transition starting at 28.1 GPa is observed and the superconductivity prevails in the pressure range up to 62.8 GPa. The upper critical magnetic field (H_{C2}) for the superconducting phase at 62.8 GPa is about 3T (see inset of Fig.1f), slightly higher than that obtained at 57 GPa (Fig.1d).

To understand the connection between the superconductivity and the WSM state in $NbIrTe_4$, we performed high-pressure measurements of the Hall resistance (R_{xy}) by sweeping the magnetic field (B), which is applied perpendicular to the *ab*-plane, from 0 to 7 T at 10 K. As shown in Fig. 2a, $R_{xy}(B)$ is negative within the pressure range investigated, indicating that electrons are the dominant charge carriers at the Fermi surface. Upon increasing pressure, the slope of $R_{xy}(B)$ becomes smaller and approaches zero at pressures above 40 GPa. These results suggest that the shrinkage of the lattice by applying pressure likely adjusts the carrier density in these two materials, leading to $R_{xy}(B)=0$ eventually.

The emergence of superconductivity in WSMs is closely associated with a suppression of *MR* [27, 28, 31]. To reveal the connection between superconductivity and positive *MR* effect in $NbIrTe_4$, we carried out *MR* measurements on our sample at 10 K in the pressure range of 1.2 - 54.8 GPa. As shown in Fig. 2b, the ambient-pressure

$NbIrTe_4$ shows a positive *MR* (*MR* (%) = 35% at 1.2 GPa, here *MR* (%) is determined by [$R(7T)$-$R(0T)$]/$R(0T)$]×100%) which can be suppressed dramatically by pressure. In the presence of superconductivity at ~27 GPa, the value of *MR* (%) is about 3.3 %.

The transport property of materials is usually influenced by the type of crystal structure. To understand why the value of *MR* does not reach zero at the critical pressure of superconducting transition, we performed high-pressure X-ray diffraction measurements. As shown in Fig. 3, all diffraction peaks gradually shift to higher angles upon increasing pressure, and the patterns can be indexed well with the orthorhombic structure ($Pmn2_1$ space group) below 24.8 GPa. At 27.5 GPa, there are two new peaks present (Fig. 3b, as indicated by stars). Although the intensity of these new peaks becomes more pronounced with elevating pressure, we are unable to determine the structure for this new phase through only two peaks. As a result, we define the new phase as the high-pressure (HP) phase in this study. These results show that the HP phase emerged from the matrix of the ambient-pressure (OR) phase and coexisted with the OR phase in the pressure range of 27.5- 40.4 GPa is responsible for the non-zero MR state and the presence of the superconducting state. When pressure is increased above 40.4 GPa, we cannot index the peaks by the OR phase, implying that the OR phase completely transforms to the HP phase at this pressure, where MR reaches zero. In the sister compound $TaIrTe_4$, the pressure-induced superconducting state is also accompanied by a lattice distortion [31]. These results suggest that the structural change from the OR phase to the HP phase are responsible for development of the superconductivity in $NbIrTe_4$. When pressure is higher than 40 GPa, the orthorhombic phase that protects the WSM state converts to HP phase completely, thus the WSM state no longer exist (Fig.3). Our results suggest that the topology of the WSM is likely not beneficial for developing the superconductivity in the pressurized $NbIrTe_4$ and $TaIrTe_4$.

We summarize our high-pressure experimental results in Fig.4. It is found that three distinct regimes can be seen in the *P-T* diagram: the Weyl semimetal (WSM) state (on the left), the mixed state of the WSM and SC states (in the middle), and the SC state (on the right). In the left regime (below the critical pressure (P_{c1}), $NbIrTe_4$ remains in the OR structure (Fig.3) and its ground state is a WSM. Within this pressure range, R_H displays a slow variation (see Supplementary Material [33]) but *MR* shows a monotonic decrease with increasing pressure (see Supplementary Material [33]). At P_{c1}, a HP phase emerges from the matrix of the OR phase, accompanied by the presence of superconductivity. Concomitantly, the value of R_H starts to approach zero, and *MR* (%) decreases to 3.3 % (see Supplementary Material [33]). In the middle of regime (27-40 GPa), a mixed state composed of the WSM state, characterized by the OR phase (Fig.3) as well as positive *MR* (Fig.2b), and the SC state is observed. In the high-pressure regime (40-57 GPa), *MR* (%) of $NbIrTe_4$ reaches zero and the OR-to-HP phase transition finishes (Fig.2b and Fig.3), implying that the ground state becomes a pure SC state.

To visualize the high-pressure behavior of these two materials, we compare the data obtained from $NbIrTe_4$ and $TaIrTe_4$ (see black squares taken from Ref. 31) in Fig.4. The critical pressure (P_{c1}) of the superconducting transition for $NbIrTe_4$ and $TaIrTe_4$ is almost same. Although the sign of their ambient-pressure R_H is different, both of the R_H

change their trend when superconductivity appears (see Supplementary Material [33]). Moreover, at the critical pressure (P_{c2}) and above, not only MR (%) of the two materials reaches zero, but also their R_H and T_c surprisingly merge into the almost same values (see Supplementary Material [33]). These results suggest that, although $NbIrTe_4$ and $TaIrTe_4$ possess dramatically different band structures at ambient pressure, the very similar high-pressure behaviors of these two materials may be attributed to that pressure assimilate their crystal and electronic structure. Our results support the previous theoretical calculations on MIrTe$_4$ (M=Ta and Nb) about that their topological band structure can be remarkably modified by the volume shrinkage [25, 39]. Because Nb and Ta have very similar ion radius but quite different mass (m_{Nb}=93, while m_{Ta}=181), these features may empower them as a unique platform to "simulate isotope effect", *i.e.* the effect of mass change on phonon and corresponding T_c, for understanding the superconducting mechanism. Subsequently, a fundamental question is raised: what is the key factor for determining the superconducting and normal states in these pressurized WSMs? and does the superconductivity found in MIrTe$_4$ (M=Nb and Ta) can fall into the unconventional superconductivity category? Moreover, it is noteworthy to ask the question about what the transport properties and the electronic state look like at the boundary of the WSM and SC states when they coexist. All calls for further investigators from theoretical and experimental sides.

In summary, we report the first observation of superconductivity in pressurized type-II WSM candidate $NbIrTe_4$, through the complementary measurements of high-pressure resistance, Hall coefficient, magnetoresistance and synchrotron X-ray diffraction. The pressure-induced superconductivity state with the transition temperature (T_c) of ~0.69 K emerges from the matrix of WSM state at 27.2 GPa. The WSM and superconducting (SC) states coexist in the pressure range of 27-40 GPa, then a pure SC state remains in the range of 40- 62.8 GPa. By comparing $NbIrTe_4$ and $TaIrTe_4$, we find a remarkably similar evolution process, from a WSM-OR phase to a SC-HP phase, in these two compounds. Intriguingly, the values of R_H, MR (%) and T_c of $NbIrTe_4$ and $TaIrTe_4$ seem the same at ~ 40 GPa and above. Our high-pressure results not only reveal the universal connection among the lattice structure, superconductivity and the band structure in these two WSMs but also demonstrate for the first time that pressure can tune these two WSMs to have the nearly identical normal and superconducting property. Such an unconventional behavior of superconductivity, independence of the mass of Nb and Ta ions, discovered in this study is of great interest and deserves investigations in the future.

Note added: Recently, a related work published in npj Quantum Materials 6, 55 (2021) was brought to our attention.

Acknowledgements

The work in China was supported by the NSF of China (Grants No. U2032214, 11888101 and 12004419) and the Strategic Priority Research Program (B) of the Chinese Academy of Sciences (Grant No. XDB25000000), the National Key Research and Development Program of China (Grant No. 2017YFA0302900 and 2017YFA0303103). We thank the support from the Users with Excellence Program of

Hefei Science Center CAS (2020HSC-UE015). Part of the work is supported by the Synergic Extreme Condition User System. S.C. and J. G. are grateful for support from the China Postdoctoral Science Foundation (E0BK111) and the Youth Innovation Promotion Association of the CAS (2019008). L.B. is supported by DOE-BES through award DE-SC0002613. The work at Los Alamos National Laboratory was supported by the Center for Integrated Nanotechnologies, and Office of Science User Facility operated for the U.S. Department of Energy, Office of Science. A portion of this work was performed at the National High Magnetic Field Laboratory, which is supported by the NSF Cooperative Agreement No. DMR-1644779, the U.S. DOE and the State of Florida.

* These authors contributed equally to this work.
†Corresponding author
llsun@iphy.ac.cn

References

[1] X. Wan, A. M. Turner, A. Vishwanath and S. Y. Savrasov. *Topological semimetal and Fermi-arc surface states in the electronic structure of pyrochlore iridates*. Physical Review B **83**, 205101 (2011).

[2] A. A. Burkov and L. Balents. *Weyl Semimetal in a Topological Insulator Multilayer*. Physical Review Letters **107**, 127205 (2011).

[3] S.-Y. Xu, I. Belopolski, N. Alidoust, M. Neupane, G. Bian, C. Zhang, R. Sankar, G.

Chang, Z. Yuan, C.-C. Lee, S.-M. Huang, H. Zheng, J. Ma, D. S. Sanchez, B. Wang, A. Bansil, F. Chou, P. P. Shibayev, H. Lin, S. Jia and M. Z. Hasan. *Discovery of a Weyl fermion semimetal and topological Fermi arcs*. Science **9**, 613 (2015).

[4] L. Lu, Z. Wang, D. Ye, L. Ran, L. Fu, J. D. Joannopoulos and M. Soljačić. *Experimental observation of Weyl points*. Science **9**, 622 (2015).

[5] L. Li, H.-H. Xie, J.-S. Zhao, X.-X. Liu, J.-B. Deng, X.-R. Hu and X.-M. Tao. *Ternary Weyl semimetal $NbIrTe_4$ proposed from first-principles calculation*. Physical Review B **96**, 024106 (2017).

[6] M. Z. Hasan and C. L. Kane. *Colloquium: Topological insulators*. Reviews of Modern Physics **82**, 3045-3067 (2010).

[7] X.-L. Qi and S.-C. Zhang. *Topological insulators and superconductors*. Reviews of Modern Physics **83**, 1057-1110 (2011).

[8] H. Weng, C. Fang, Z. Fang, B. A. Bernevig and X. Dai. *Weyl Semimetal Phase in Noncentrosymmetric Transition-Metal Monophosphides*. Physical Review X **5**, 011029 (2015).

[9] G. Xu, H. Weng, Z. Wang, X. Dai and Z. Fang. *Chern Semimetal and the Quantized Anomalous Hall Effect in $HgCr_2Se_4$*. Physical Review Letters **107**, 186806 (2011).

[10] S.-M. Huang, S.-Y. Xu, I. Belopolski, C.-C. Lee, G. Chang, B. Wang, N. Alidoust, G. Bian, M. Neupane, C. Zhang, S. Jia, A. Bansil, H. Lin and M. Z. Hasan. *A Weyl Fermion semimetal with surface Fermi arcs in the transition metal monopnictide TaAs class*. Nature Communications **6**, 7373 (2015).

[11] A. A. Soluyanov, D. Gresch, Z. Wang, Q. Wu, M. Troyer, X. Dai and B. A.

Bernevig. *Type-II Weyl semimetals*. Nature **527**, 495-498 (2015).

[12] L. X. Yang, Z. K. Liu, Y. Sun, H. Peng, H. F. Yang, T. Zhang, B. Zhou, Y. Zhang, Y. F. Guo, M. Rahn, D. Prabhakaran, Z. Hussain, S. K. Mo, C. Felser, B. Yan and Y. L. Chen. *Weyl semimetal phase in the non-centrosymmetric compound TaAs*. Nature Physics **11**, 728-732 (2015).

[13] B. Q. Lv, H. M. Weng, B. B. Fu, X. P. Wang, H. Miao, J. Ma, P. Richard, X. C. Huang, L. X. Zhao, G. F. Chen, Z. Fang, X. Dai, T. Qian and H. Ding. *Experimental Discovery of Weyl Semimetal TaAs*. Physical Review X **5**, 031013 (2015).

[14] Y. Sun, S.-C. Wu, M. N. Ali, C. Felser and B. Yan. *Prediction of Weyl semimetal in orthorhombic $MoTe_2$*. Physical Review B **92**, 161107 (2015).

[15] K. Koepernik, D. Kasinathan, D. V. Efremov, S. Khim, S. Borisenko, B. Büchner and J. van den Brink. *$TaIrTe_4$: A ternary type-II Weyl semimetal*. Physical Review B **93**, 201101 (2016).

[16] G. Autès, D. Gresch, M. Troyer, A. A. Soluyanov and O. V. Yazyev. *Robust Type-II Weyl Semimetal Phase in Transition Metal Diphosphides XP_2 (X=Mo, W)*. Physical Review Letters **117**, 066402 (2016)

[17] X. Huang, L. Zhao, Y. Long, P. Wang, D. Chen, Z. Yang, H. Liang, M. Xue, H. Weng, Z. Fang, X. Dai and G. Chen. *Observation of the Chiral-Anomaly-Induced Negative Magnetoresistance in 3D Weyl Semimetal TaAs*. Physical Review X **5**, 031023 (2015).

[18] A. A. Zyuzin and A. A. Burkov. *Topological response in Weyl semimetals and the chiral anomaly*. Physical Review B **86**, 115133 (2012).

[19] A. C. Potter, I. Kimchi and A. Vishwanath. *Quantum oscillations from surface Fermi arcs in Weyl and Dirac semimetals*. Nature Communications **5**, 5161 (2014).

[20] Y. Qi, P. G. Naumov, M. N. Ali, C. R. Rajamathi, W. Schnelle, O. Barkalov, M. Hanfland, S.-C. Wu, C. Shekhar, Y. Sun, V. Süß, M. Schmidt, U. Schwarz, E. Pippel, P. Werner, R. Hillebrand, T. Förster, E. Kampert, S. Parkin, R. J. Cava, C. Felser, B. Yan and S. A. Medvedev. *Superconductivity in Weyl semimetal candidate $MoTe_2$*. Nature Communications **7**, 11038 (2016).

[21] F. C. Chen, X. Luo, R. C. Xiao, W. J. Lu, B. Zhang, H. X. Yang, J. Q. Li, Q. L. Pei, D. F. Shao, R. R. Zhang, L. S. Ling, C. Y. Xi, W. H. Song and Y. P. Sun. *Superconductivity enhancement in the S-doped Weyl semimetal candidate $MoTe_2$*. Applied Physics Letters **108**, 162601 (2016).

[22] L. Zhu, Q.-Y. Li, Y.-Y. Lv, S. Li, X.-Y. Zhu, Z.-Y. Jia, Y. B. Chen, J. Wen and S.-C. Li. *Superconductivity in Potassium-Intercalated T_d-WTe_2*. Nano Letters **18**, 6585-6590 (2018).

[23] V. Fatemi, S. Wu, Y. Cao, L. Bretheau, Q. D. Gibson, K. Watanabe, T. Taniguchi, R. J. Cava and P. Jarillo-Herrero. *Electrically tunable low-density superconductivity in a monolayer topological insulator*. Science **362**, 926 (2018).

[24] E. Sajadi, T. Palomaki, Z. Fei, W. Zhao, P. Bement, C. Olsen, S. Luescher, X. Xu, J. A. Folk and D. H. Cobden. *Gate-induced superconductivity in a monolayer topological insulator*. Science **362**, 922 (2018).

[25] X. Zhou, Q. Liu, Q. Wu, T. Nummy, H. Li, J. Griffith, S. Parham, J. Waugh, E. Emmanouilidou, B. Shen, O. V. Yazyev, N. Ni and D. Dessau. *Coexistence of tunable

Weyl points and topological nodal lines in ternary transition-metal telluride $TaIrTe_4$. Physical Review B **97**, 241102 (2018).

[26] R. Schönemann, Y.-C. Chiu, W. Zheng, V. L. Quito, S. Sur, G. T. McCandless, J. Y. Chan and L. Balicas. *Bulk Fermi surface of the Weyl type-II semimetallic candidate $NbIrTe_4$*. Physical Review B **99**, 195128 (2019).

[27] D. Kang, Y. Zhou, W. Yi, C. Yang, J. Guo, Y. Shi, S. Zhang, Z. Wang, C. Zhang, S. Jiang, A. Li, K. Yang, Q. Wu, G. Zhang, L. Sun and Z. Zhao. *Superconductivity emerging from a suppressed large magnetoresistant state in tungsten ditelluride*. Nature Communications **6**, 7804 (2015).

[28] X.-C. Pan, X. Chen, H. Liu, Y. Feng, Z. Wei, Y. Zhou, Z. Chi, L. Pi, F. Yen, F. Song, X. Wan, Z. Yang, B. Wang, G. Wang and Y. Zhang. *Pressure-driven dome-shaped superconductivity and electronic structural evolution in tungsten ditelluride*. Nature Communications **6**, 7805 (2015).

[29] Z. Guguchia, F. von Rohr, Z. Shermadini, A. T. Lee, S. Banerjee, A. R. Wieteska, C. A. Marianetti, B. A. Frandsen, H. Luetkens, Z. Gong, S. C. Cheung, C. Baines, A. Shengelaya, G. Taniashvili, A. N. Pasupathy, E. Morenzoni, S. J. L. Billinge, A. Amato, R. J. Cava, R. Khasanov and Y. J. Uemura. *Signatures of the topological $s+-$ superconducting order parameter in the type-II Weyl semimetal T_d-$MoTe_2$*. Nature Communications **8**, 1082 (2017).

[30] Y. Li, Q. Gu, C. Chen, J. Zhang, Q. Liu, X. Hu, J. Liu, Y. Liu, L. Ling, M. Tian, Y. Wang, N. Samarth, S. Li, T. Zhang, J. Feng and J. Wang. *Nontrivial superconductivity in topological $MoTe_{2-x}S_x$ crystals*. Proceedings of the National Academy of Sciences

115, 9503 (2018).

[31] S. Cai, E. Emmanouilidou, J. Guo, X. Li, Y. Li, K. Yang, A. Li, Q. Wu, N. Ni and L. Sun. *Observation of superconductivity in the pressurized Weyl-semimetal candidate* $TaIrTe_4$. Physical Review B **99**, 020503 (2019).

[32] Y. Xing, Z. Shao, J. Ge, J. Luo, J. Wang, Z. Zhu, J. Liu, Y. Wang, Z. Zhao, J. Yan, D. Mandrus, B. Yan, X.-J. Liu, M. Pan and J. Wang. *Surface superconductivity in the type II Weyl semimetal* $TaIrTe_4$. National Science Review **7**, 579-587 (2020).

[33] *Supplemental Material for the high pressure experimental details and extended results*.

[34] H. K. Mao, J. Xu and P. M. Bell. *Calibration of the ruby pressure gauge to 800 kbar under quasi-hydrostatic conditions*. Journal of Geophysical Research: Solid Earth 91, 4673-4676 (1986).

[35] L. Sun, A. L. Ruoff and G. Stupian. *Convenient optical pressure gauge for multimegabar pressures calibrated to 300GPa*. Applied Physics Letters 86, 014103 (2004).

[36] Y. Akahama and H. Kawamura. *Pressure calibration of diamond anvil Raman gauge to 310GPa*. Journal of Applied Physics 100, 043516 (2006).

[37] Y. Liu, Q. Gu, Y. Peng, S. Qi, N. Zhang, Y. Zhang, X. Ma, R. Zhu, L. Tong, J. Feng, Z. Liu and J.-H. Chen. *Raman Signatures of Broken Inversion Symmetry and In-Plane Anisotropy in Type-II Weyl Semimetal Candidate* $TaIrTe_4$. Advanced Materials **30**, 1706402 (2018).

[38] N. R. Werthamer, E. Helfand and P. C. Hohenberg. *Temperature and Purity*

Dependence of the Superconducting Critical Field, H_{c2}. III. Electron Spin and Spin-Orbit Effects. Physical Review **147**, 295-302 (1966).

[39] J. Liu, H. Wang, C. Fang, L. Fu and X. Qian. *van der Waals Stacking-Induced Topological Phase Transition in Layered Ternary Transition Metal Chalcogenides*. Nano Letters **17**, 467-475 (2017).

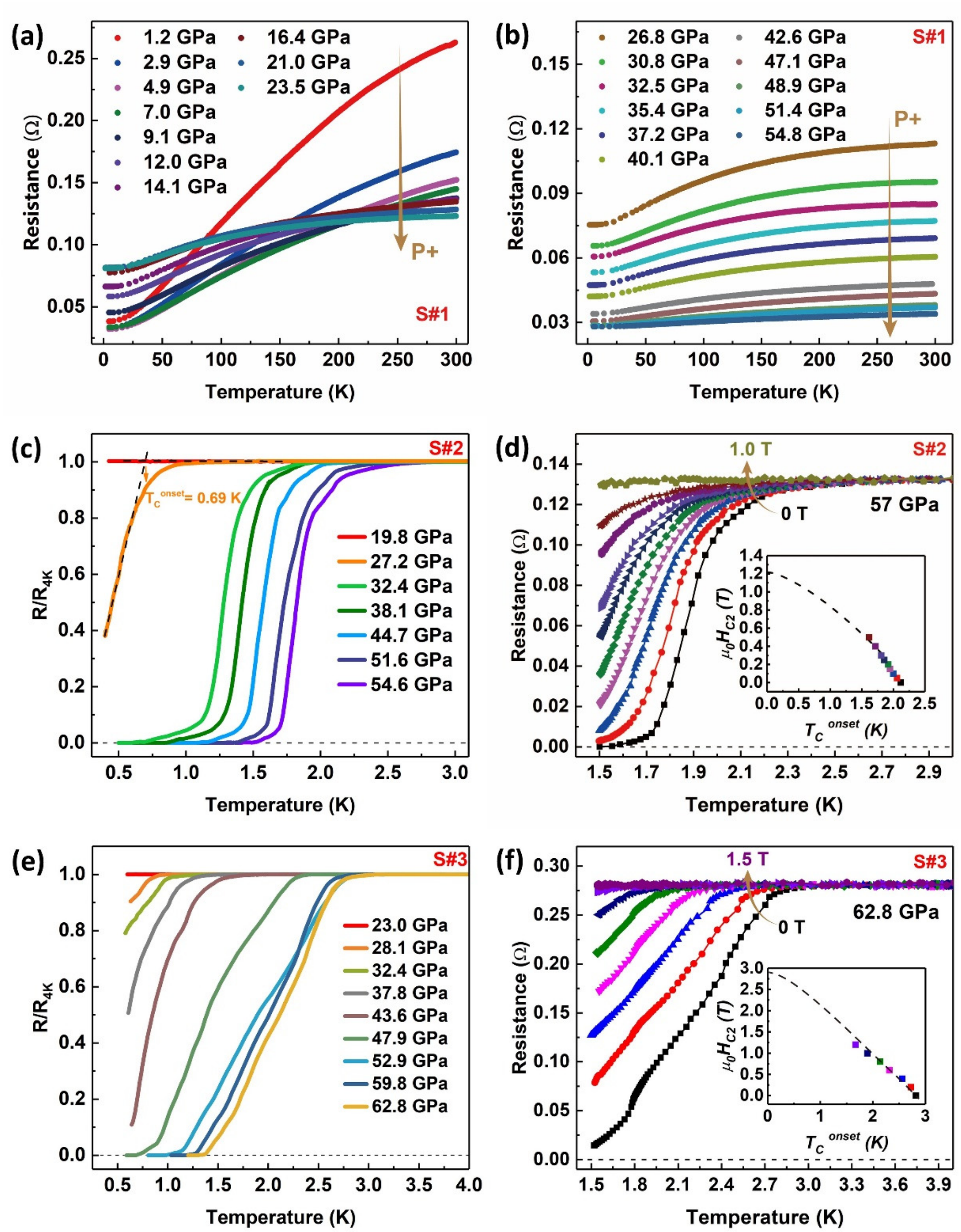

Figure 1. Temperature-dependence of electrical resistance at different pressures and magnetic fields. (a) and (b) The resistance as a function of temperature for the sample 1 (S#1) measured over the range of 1.5-300 K at different pressures. (c) and (e) The

resistance versus temperature for the sample 2 (S#2) and the sample 3 (S#3) measured in the range of 0.35-4K at different pressures, showing the superconducting transition. (d) and (f) Magnetic field dependence of the superconducting transition temperature measured at 57 GPa and at 62.8 GPa for the S#2 and S#3, respectively. The insets of Fig. 1d and 1f show the dependence of upper critical field.

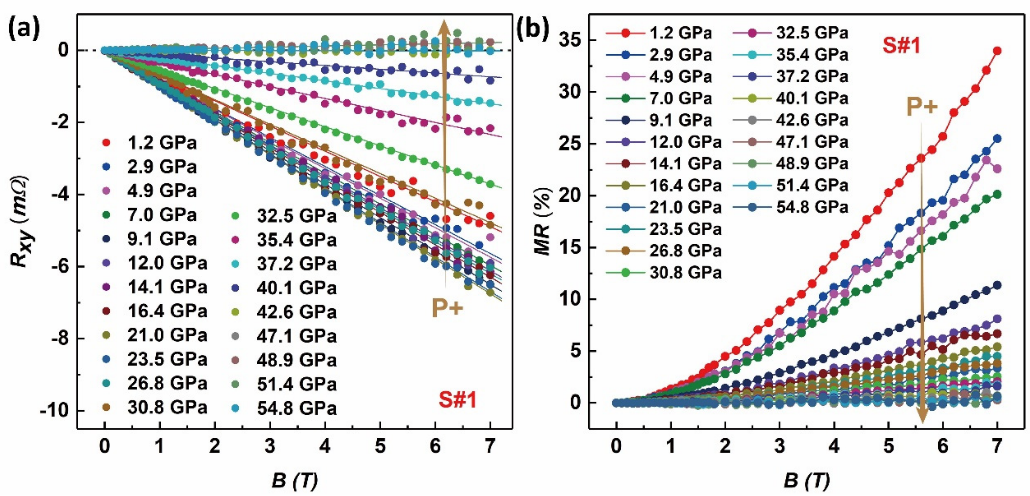

Figure 2. Results of Hall and magnetoresistance obtained from $NbIrTe_4$. (a) Hall resistance (R_{xy}) as a function of magnetic field at different pressures, displaying that $R_{xy}(B)$ exhibits a slow change below 26.8 GPa, then increases above this pressure and tends to zero upon further compression. (b) Magnetic field dependence of magnetoresistance (*MR*(%) for pressures ranging from 1.2 GPa to 54.8 GPa (here *MR*(%)=[*R*(7T)-*R*(0T)]/*R*(0T) ×100%), showing that *MR*(%) decreases with increasing pressure.

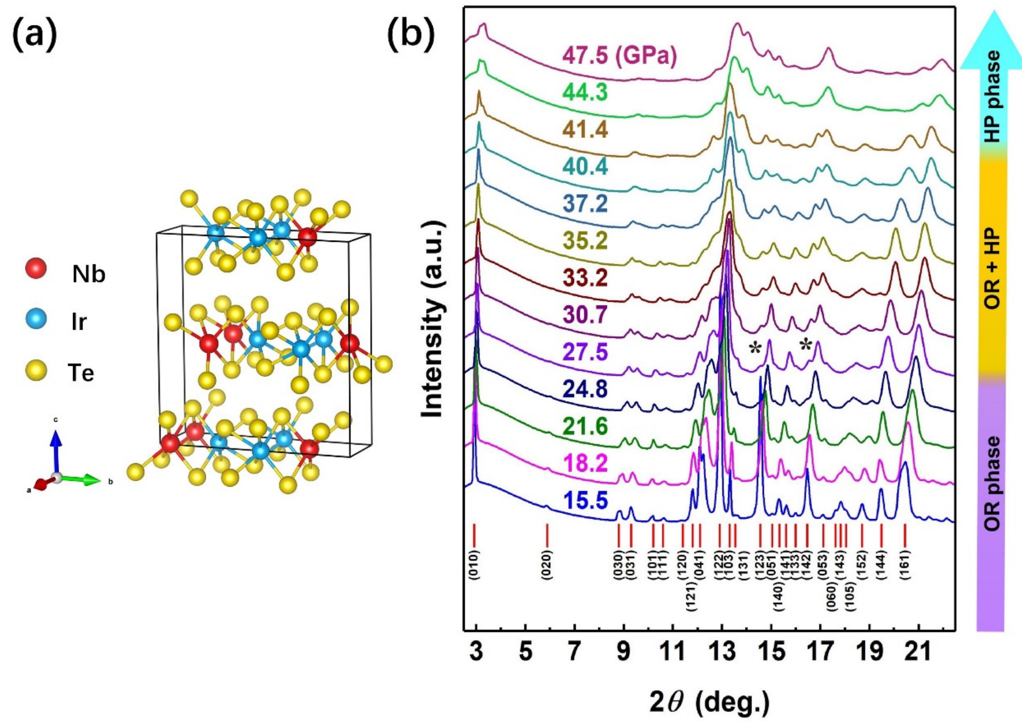

Figure 3. (a) Schematic crystal structure of $NbIrTe_4$. (b) X-ray diffraction patterns collected at different pressures. In the range of 15-27 GPa, the sample remains OR phase (see violet regime), while, in the range of 27.5-40.4 GPa, it hosts a mixed phase composed of OR and HP phases (see the orange regime). Upon further compression, the sample possesses a pure HP phase (see the cyan regime).

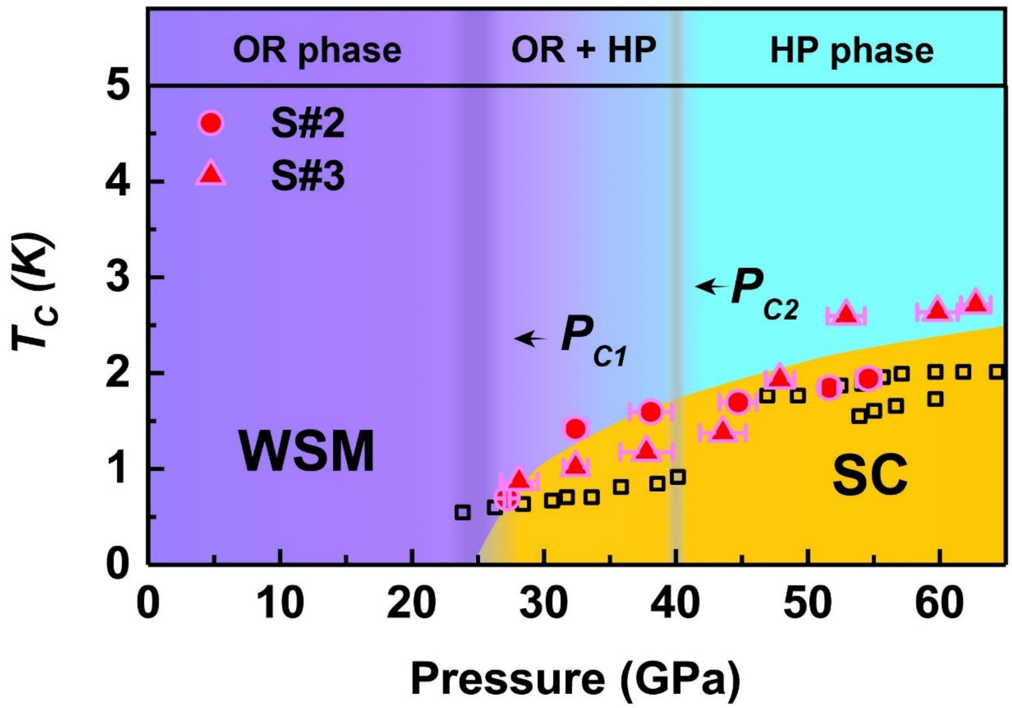

Figure 4. Pressure $-T_c$ phase diagram with structure information for $NbIrTe_4$. The data of $TaIrTe_4$ (see black squares taken from Ref. 31) is included for comparison. WSM and SC represent Weyl semimetal and superconducting states, respectively.